Article

INF2-Mediated Severing through Actin Filament Encirclement and Disruption

Pinar S. Gurel,[1] Peng Ge,[2] Elena E. Grintsevich,[3] Rui Shu,[1] Laurent Blanchoin,[4] Z. Hong Zhou,[2,5] Emil Reisler,[3,5] and Henry N. Higgs[1,*]

[1]Department of Biochemistry, Geisel School of Medicine at Dartmouth, Hanover, NH 03755, USA
[2]Electron Imaging Center for NanoMachines and Department of Microbiology, Immunology, and Molecular Genetics, UCLA School of Medicine, Los Angeles, CA 90095, USA
[3]Department of Chemistry and Biochemistry, UCLA, Los Angeles, CA 90095, USA
[4]CEA, iRTSV, Laboratoire Physiologie Cellulaire & Végétale, CNRS, UMR 5168, Université Joseph Fourier-Grenoble 1, 38054 Grenoble, France
[5]Molecular Biology Institute, UCLA, Los Angeles, CA 90095, USA

Summary

Background: INF2 is a formin protein with the unique ability to accelerate both actin polymerization and depolymerization, the latter requiring filament severing. Mutations in INF2 lead to the kidney disease focal segmental glomerulosclerosis (FSGS) and the neurological disorder Charcot-Marie Tooth disease (CMTD).
Results: Here, we compare the severing mechanism of INF2 with that of the well-studied severing protein cofilin. INF2, like cofilin, binds stoichiometrically to filament sides and severs in a manner that requires phosphate release from the filament. In contrast to cofilin, however, INF2 binds ADP and ADP-P_i filaments equally well. Furthermore, two-color total internal reflection fluorescence (TIRF) microscopy reveals that a low number of INF2 molecules, as few as a single INF2 dimer, are capable of severing, while measurable cofilin-mediated severing requires more extensive binding. Hence, INF2 is a more potent severing protein than cofilin. While a construct containing the FH1 and FH2 domains alone has some severing activity, addition of the C-terminal region increases severing potency by 40-fold, and we show that the WH2-resembling DAD motif is responsible for this increase. Helical 3D reconstruction from electron micrographs at 20 Å resolution provides a structure of filament-bound INF2, showing that the FH2 domain encircles the filament.
Conclusions: We propose a severing model in which FH2 binding and phosphate release causes local filament deformation, allowing the DAD to bind adjacent actin protomers, further disrupting filament structure.

Introduction

The actin cytoskeleton plays roles in many cellular processes, including migration, cytokinesis, phagocytosis, and organelle dynamics [1]. The diversity of actin-based processes arises from modulation of filament assembly and organization by specific actin-binding proteins, including formins. Formins use their dimeric formin homology 2 (FH2) domains to nucleate

*Correspondence: henry.higgs@dartmouth.edu

new filaments, and they remain at the fast-growing barbed ends of these filaments as they elongate [2, 3]. The FH1 domain accelerates elongation through its interaction with the actin monomer binding protein profilin [4]. The diversity of formins, including 15 mammalian proteins, provides the potential for extensive variation in assembly of actin-based structures [1, 5].

Several formins also interact with actin through C-terminal sequences, which provide additional abilities to influence actin dynamics [6, 7]. The vertebrate formin INF2 is particularly noteworthy, in that its long C-terminal region (300 amino acids) allows acceleration of both actin polymerization and depolymerization [8]. INF2's C terminus contains a diaphanous autoregulatory domain (DAD) close to the FH2 domain that binds actin monomers, similar to WASp homology 2 (WH2) motifs [8].

In cells, INF2 exists as two isoforms varying at their extreme C termini. The INF2-nonCAAX variant is cytosolic, it and plays a role in maintaining Golgi integrity [9] and in directed vesicular transport [10, 11]. The INF2-CAAX variant is tightly bound to endoplasmic reticulum (ER) and acts in mitochondrial fission by assembling highly transient actin filaments at the ER/mitochondrial interface [12, 13]. These functions are medically important, since INF2 mutations lead to the kidney disease focal segmental glomerulosclerosis (FSGS) and the neuropathy Charcot-Marie Tooth disease (CMTD) [14, 15].

To understand INF2's physiological roles, it is critical to clarify its effects on actin biochemically. Prior work suggested that INF2-mediated filament depolymerization requires a severing step that is dependent on ATP hydrolysis and phosphate release from actin protomers in the filament [8]. The need for phosphate release is not unique to INF2. Cofilin, a well-characterized severing protein, binds and severs filaments mainly after phosphate release [16–18]. Under both cellular and experimental conditions, ATP hydrolysis (0.3 s^{-1}) and phosphate release (0.002 s^{-1}) lag significantly behind polymerization (10 $\mu M^{-1}s^{-1}$), resulting in preferential cofilin binding to aged filament segments [19–22]. Upon binding, cofilin changes filament twist, creating strain at the boundary between cofilin-decorated and undecorated regions [23–25]. Cofilin binding also accelerates phosphate release from adjacent actin subunits, rendering binding cooperative [20, 21, 23, 26, 27].

We show that INF2's severing mechanism is distinct from that of cofilin. INF2 binds stoichiometrically to filament sides in a phosphate-independent manner. This binding step consists of opening the FH2 dimer and then encirclement of the filament. INF2 binds at discrete sites throughout the filament length and, in a step dependent on phosphate release, severs at sites of binding. We propose a model for INF2-mediated severing involving filament disruption both by FH2 binding and DAD insertion.

Results

INF2 Severs along the Length of the Filament
Previous data suggested that INF2 severs filaments, but did not show direct evidence for severing nor reveal the position of binding or severing events [8]. We used a two-color total internal reflection fluorescence (TIRF) microscopy assay
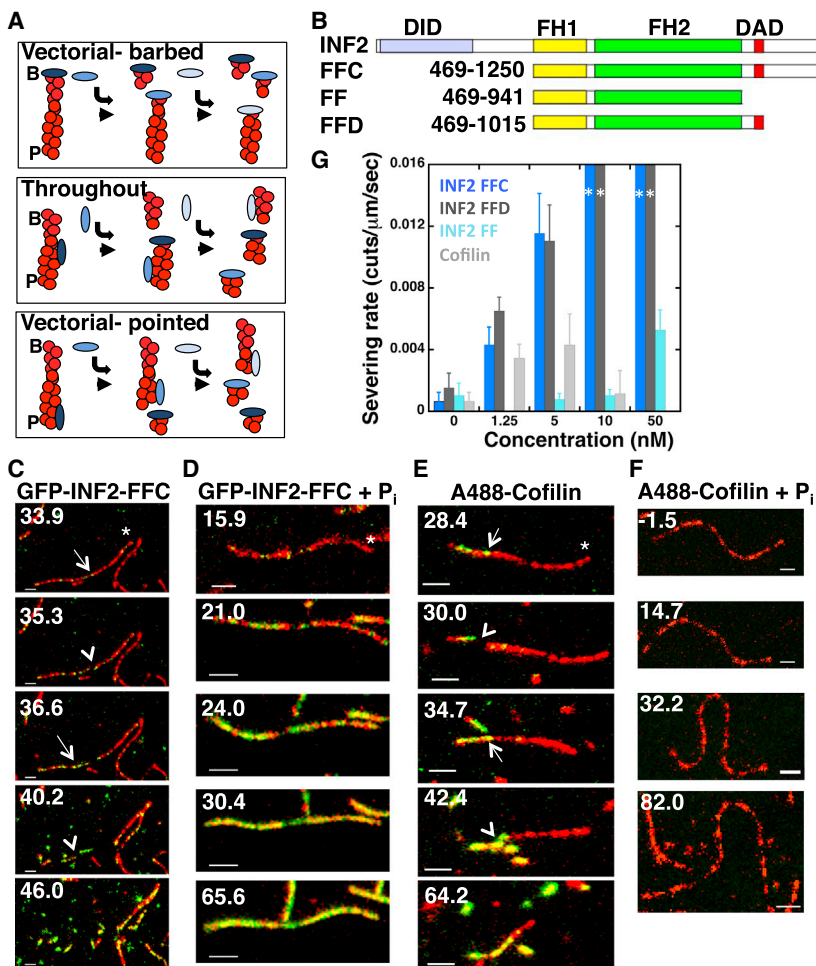
Figure 1. INF2 Severs Filaments throughout Their Length

(A) Three models for INF2 severing. (1) Vectorial barbed: INF2 binds barbed end and removes a short filament fragment from that end. (2) Throughout: INF2 binds and severs at random positions along filament side, creating two longer fragments. INF2 subsequently binds the newly created barbed end. (3) Vectorial pointed: INF2 binds and severs at ADP-actin protomers near pointed end. B, barbed; P, pointed.

(B) Bar diagram showing human INF2 constructs (lengths in amino acids). DID, diaphanous inhibitory domain; FH1, formin homology 1; FH2, formin homology 2; DAD, diaphanous autoregulatory domain.

(C) Two-color simultaneous TIRF microscopy montage of GFP-INF2-FFC (10 nM) binding actin filament sides (1 μM, 20% TAMRA initially) and severing on DDS/F127-treated slides. Time indicates seconds after INF2 addition (and washout of actin monomers). Asterisk, barbed end; arrow, GFP punctum correlated with severing; arrowhead, severing event. Scale bar, 2 μm. See also Movie S1.

(D) As in (C) but with GFP-INF2-FFC (100 nM) + 10 mM phosphate. See also Movie S2.

(E) As in (C) but with A488-cofilin (5 nM). See also Movie S3.

(F) As in (C) but with A488-cofilin (100 nM) + 10 mM phosphate. See also Movie S4.

(G) Concentration dependence of severing rate for INF2-FFC, INF2-FFD, INF2-FF, and cofilin on DDS/F127-treated slides. n values were as follows: 18, 50, 48 severing events (7, 6, 6 filaments) for 0, 1.25, and 5 nM INF2-FFC (dark blue); 15, 29, 40 events (6, 5, 7 filaments) for 0, 1.25, and 5 nM INF2-FFD (dark gray); 9, 14, 15, 23 events (5, 6, 5, 5 filaments) for 0, 5, 10, and 50 nM INF2-FF (light blue); 18, 42, 21, 4 events (7, 7, 5, 7 filaments) for 0, 1.25, 5, and 10 nM cofilin (light gray). For 10 and 50 nM INF2-FFC and INF2-FFD, ten and six filaments were examined respectively, but severing events were too rapid to quantify (depicted by dark blue or dark gray bar to the maximum rate). The highest concentrations tested (1 μM INF2-FFC and 500 nM INF2-FFD) produced similar results. See also Figure S1 and Movies S1, S2, S3, and S4.

containing fluorescently labeled actin and GFP-INF2-FFC (containing the FH1, FH2, and C-terminal regions; Figure 1) to visualize INF2 severing events in real time. Due to INF2's potent actin nucleation activity, we first polymerized actin alone for a fixed time before washing out the remaining monomers and adding GFP-INF2-FFC. This procedure allows the production of longer filaments, more amenable to severing analysis than the short filaments generated by INF2-mediated nucleation.

We anticipated three possible results regarding severing position (Figure 1A): (1) severing occurs vectorially from the barbed end, due to INF2's barbed-end binding; (2) severing occurs throughout the filament length, at some distance from either filament end; or (3) severing occurs predominantly toward the pointed end, due to the need for phosphate release [8]. Our results support model (2), with severing occurring at many positions along the filament (Figure 1C and Movie S1 available online). This tendency to sever throughout the filament is independent of the TIRF coverslip preparation technique and occurs with unlabeled INF2-FFC as well as with GFP-INF2-FFC (Figure S1).

We compared severing by INF2 to that by cofilin, whose severing mechanism is better understood. Cofilin-mediated severing occurs predominately at boundaries between cofilin-

bound and unbound regions (Figure 1E and Movie S3) [21]. Accordingly, the concentration dependence of cofilin severing is bimodal, with reduced severing at low and high cofilin concentrations [28–30]. Cofilin displays similar severing tendency in our system (Figures 1G and S1). In contrast, INF2-mediated severing frequency increases continuously with INF2 concentration (Figure 1G) until all filaments are reduced to unresolvable lengths. Deletion mutagenesis of the C terminus shows that inclusion of DAD alone is sufficient for robust severing activity, with INF2-FFC and INF2-FFD constructs displaying similar severing rates (Figures 1G and S1). Removal of the entire C terminus causes a dramatic decrease in severing activity for the resulting INF2-FF construct, with no measurable severing at lower concentrations and a severing rate at 50 nM approaching that of 1.25 nM FFC (Figures 1G and S1). Additionally, INF2-FFC severing activity is significantly more potent than cofilin's at all concentrations tested (Figure 1G).

INF2 Binds throughout the Filament but Severs Preferentially Toward the Pointed End

The TIRF assays also show that GFP-INF2-FFC binds filament sides, similar to cofilin. Previously, we showed that the presence of phosphate inhibits INF2-mediated severing [8], suggesting that ATP hydrolysis and phosphate release by actin
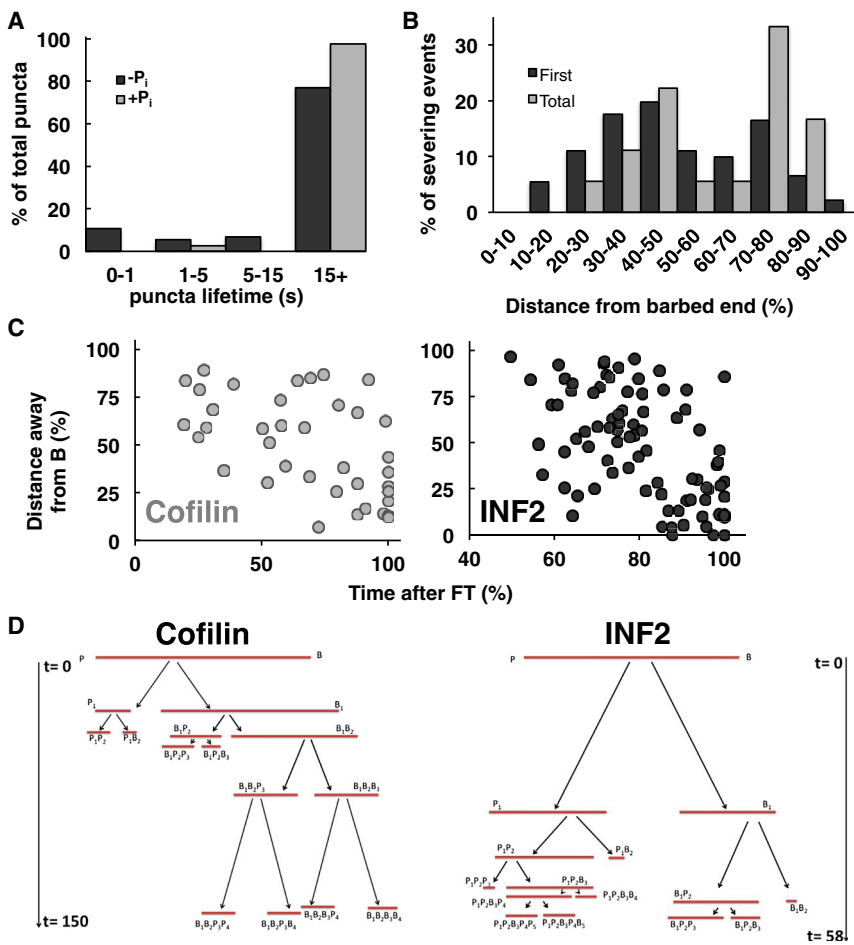
A

B

Figure 2. INF2 Binds throughout the Filament but Severs toward the Pointed End

(A) Lifetimes of filament-bound puncta as in (C) and (D). More than 15 s indicates puncta that did not dissociate during the observation period (180 s). n = 74 and 39 puncta (13 and six filaments) in the absence and presence of phosphate, respectively.

(B) Histogram of severing positions for GFP-INF2-FFC (5–20 nM) on DDS/F127-treated slides. Eighteen filaments (91 severing events) were quantified (average length 12.3 μm, range 5.83–24.22 μm at time = 0). Barbed-end fragments were measured as a percentage of total filament length.

C

(C) Correlation of time of severing with respect to distance from original barbed end (as a percentage of original length). n = 80 and 38 severing events (11 and seven filaments) for GFP-INF2-FFC and A488-cofilin, respectively. Filaments were 12.5 and 7.86 μm mean length (range 6.49–21.59 and 4.55–11.05 μm) prior to INF2-FFC or cofilin addition, respectively. Severing events were observed for 57.5–112.3 and 68.6–170.8 s after addition of INF2 or cofilin, respectively. Note that the x axis scale is different between INF2 and cofilin.

D

(D) Tree map diagraming severing events on individual filaments with time (s) on the y axis. t = 0 denotes time of cofilin or INF2-FFC addition. B and P denote barbed and pointed ends. Severed filament fragments are named based on severing history with subscripts denoting lineage (B_1 being the first barbed-end fragment, B_1B_2 being the second barbed-end fragment originating from the first barbed-end fragment, and so forth). Original filament lengths were 11.1 (cofilin) and 13.6 μm (INF2). Time and sizes are drawn to scale. See also Figure S2 for additional examples from (D).

protomers in the filament is necessary for severing. Phosphate inhibits cofilin-mediated severing by decreasing cofilin's side-binding affinity significantly (Figure 1F and Movie S4) [16]. In contrast, GFP-INF2-FFC still binds filaments in the presence of phosphate (Figure 1D and Movie S2). To confirm and extend this result, we used actin filament cosedimentation assays. INF2-FFC binds filaments with comparable affinity in the presence and absence of phosphate (Figure S1 and Table S1). In addition, INF2 binding saturates at a 1:1 ratio (INF2 monomer: actin monomer) in both cases (Figure S1 and Table S1). INF2-FF binds with 5-fold lower affinity, but still reaches saturation (data not shown). We conclude that, in clear contrast to cofilin, INF2 binds filament sides in a manner independent of phosphate release, suggesting that phosphate release allows severing downstream of INF2 binding.

We used two-color TIRF microscopy to examine the pattern of GFP-INF2-FFC side binding. Initially, GFP-INF2-FFC binds at discrete sites without preference for a particular filament end in the presence or absence of phosphate (Figures 1C, 1D, and S2). Most puncta are stably bound, with 77% and 97% of puncta remaining throughout the 3 min acquisition time (Figure 2A). In the presence of phosphate, progressive addition of puncta results in full filament saturation with GFP-INF2-FFC at a uniform intensity (Figure 1D). In the absence of phosphate, saturating GFP-INF2-FFC occurs in some segments, but is largely counteracted by severing (Figure 1C).

The distribution of GFP-INF2-FFC puncta throughout the filament supports our observation that INF2-mediated severing

is not vectorial. Quantification of severing events with respect to original or newly created barbed ends further shows that severing occurs throughout the filament (Figures 2B and S2). However, our results reported previously and in this publication, showing that severing depends upon phosphate release, suggest that severing should occur preferentially toward the pointed end. We analyzed severing positional kinetics in more detail to determine the distance of a severing event from the original filament barbed end as a function of time after INF2 addition to the assay. This analysis shows that both INF2 and cofilin display preferences for severing nearer the pointed end at early time points, with events closer to the barbed end increasing at later time points (Figure 2C). Tracking the progressive severing of individual filaments reveals a similar pattern, but also shows that INF2-mediated severing is less vectorial than cofilin, with some initial severing events occurring more toward the barbed end (Figures 2D and S2). Severing often occurs more rapidly than would be predicted from ATP hydrolysis and phosphate release rate constants (Figure S2), which might imply that INF2 binding could enhance phosphate release locally.

INF2 Binds Filament Sides as Single Dimers and Severs at Binding Sites

Having established that GFP-INF2-FFC binds filament sides as discrete puncta, we next examined the relationship between INF2 binding and filament severing in more detail by asking two questions: how many INF2 molecules are required for
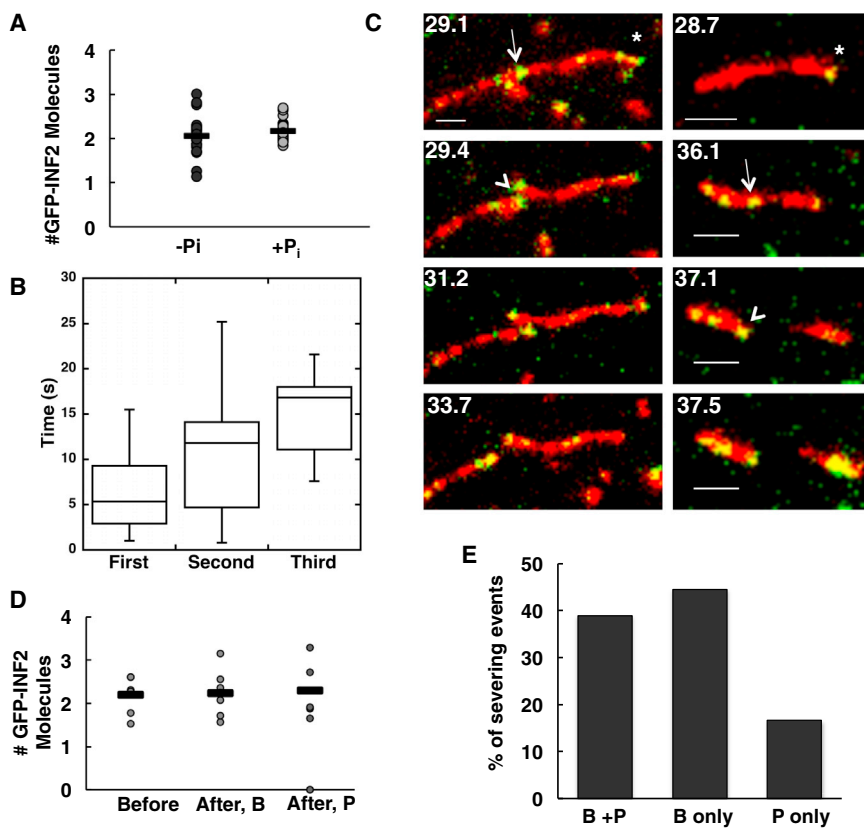
Figure 3. INF2 Binds Filament Sides as Single Dimers and Severs at Binding Sites

(A) Number of GFP-INF2-FFC molecules localized at diffraction-limited puncta (n = 28 and 25 puncta [eight and six filaments] in the absence and presence of phosphate, respectively). Averages (bars) are 2.06 and 2.17 molecules in the absence and presence of phosphate, respectively.

(B) Box-and-whisker quantification of severing time after punctum binding for first, second, and third severing events. Line, mean; box, values 25%–75% of totals; whiskers, full range of values. n = 14, 9, and 5 events.

(C) Two examples of severing at sites where an apparent single GFP-INF2-FFC dimer (green) is bound to TAMRA-actin (red). Asterisk, barbed end; arrow, punctum correlated with severing; arrowhead, severing event. Left: GFP-INF2 puncta present at both new barbed and pointed ends after severing. Right: GFP-INF2 punctum only at new barbed end after severing. Scale bar, 2 μm. See also Movies S5 and S6.

(D) Distribution of GFP-INF2-FFC localization after severing for events occurring at sites where two GFP-INF2-FFCs were located prior to severing. "After, B," new barbed end; "After, p," new pointed end. Bars represent the averages from seven events. Note: two events result in punctum localization at only new barbed end.

(E) Localization of puncta after a severing event with respect to newly created barbed or pointed ends. All severing events are included, regardless of the number of GFP-INF2-FFC molecules present before the event. n = 18 filaments.

See also Figure S3 and Movies S5 and S6.

severing, and how rapidly does severing occur after INF2 binding? To calibrate GFP-INF2-FFC fluorescence, we first monitored GFP intensity on the barbed ends of elongating filaments, assuming dimeric GFP-INF2-FFC binding to the barbed end, since INF2 is dimeric in solution [8], like other formins [31]. Barbed-end GFP intensity varies ∼2-fold over time (Figure S3), possibly due to varying distance from the coverslip or GFP flickering. Using this calibration, the majority of diffraction-limited side-bound puncta appear to represent GFP-INF2-FFC dimers in the absence or presence of phosphate (Figure 3A).

We next investigated the kinetic relationship between GFP-INF2-FFC binding and severing, quantifying initial severing events in greater detail than subsequent events because individual puncta were more clearly discernable at early time points. Severing typically occurs at sites where an INF2 punctum is present (18 out of 19 events), but there is a significant delay (6.5 ± 4.5 s) between binding and severing (Figure 3B). Often, severing does not occur at the first binding site, and on average seven ± three puncta bind to the filament prior to the first severing event. For subsequent severing events, GFP-INF2-FFC is always present at the severing site, either as a punctum or as a uniform coating on that region of the filament (n = 14 severing events, 11 filaments), with INF2 arriving on average 10.7 ± 7.6 and 15 ± 5 s prior to severing for second and third events, respectively (Figure 3B).

The number of GFP-INF2-FFC molecules present at the severing site is variable, but appears to be as low as two (or one INF2 dimer; Figure 3D), although variability in the calibration standard (Figure S3) introduces some uncertainty here. After severing, INF2 remains at the new barbed end (Figure 3C,

right; Figure 3E; and Movie S5). However, in several cases, INF2 is also present at the new pointed end immediately after severing (Figure 3C, left; Figures 3D and 3E; and Movie S6), suggesting that a second INF2 dimer may have added during severing, although we were unable to observe this directly. When all severing events are analyzed, INF2 remains at the new barbed end 83% of the time, with 47% also having INF2 at the new pointed end (Figure 3E). In a minority of cases, INF2 is only at the new pointed end (Figure 3E).

INF2's FH2 Domain Encircles the Filament

Our results show that INF2 binds filament sides and dissociates with an extremely slow off rate. How does this binding occur? FH2 domains are dimeric and adopt a "donut"-like conformation, with barbed-end-interacting residues on the inner face of the donut [31, 32]. We expected that INF2's FH2 domain might bind filament sides through two possible mechanisms: (1) by encircling the filament and binding through residues on the inner face of the donut, similar to those used at the barbed end, or (2) by binding the filament side through residues on the outer face of the donut (Figure 4A).

If model (1) is correct and INF2 encircles the filament, the INF2 FH2 dimer might be able to dissociate because it is unlikely that the dimer could "slide" along the filament over micron distances once bound to the barbed end. To test INF2 FH2 dimer dissociation, we conducted sedimentation velocity experiments using purified GFP-INF2-FF and unlabeled INF2-FF and detecting fluorescence at 490 nm to follow the GFP (Figure 4B). GFP-INF2-FF alone has a sedimentation coefficient of approximately 5.4 S (Figure 4C, Table 1). In the presence of excess unlabeled INF2-FF, the sedimentation
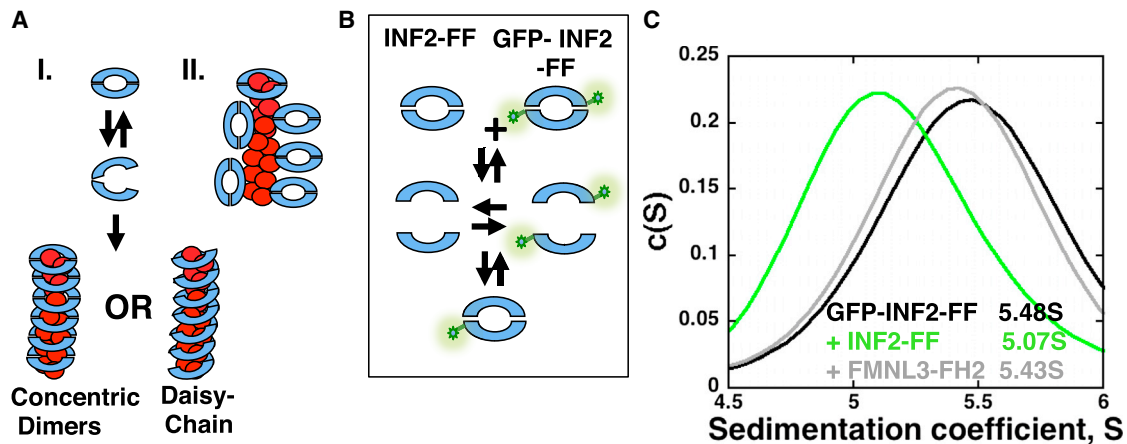
Figure 4. INF2 Is a Dissociating Dimer that Binds Stoichiometrically to Filament Sides

(A) Two models for INF2 binding filament sides. (I) FH2 dimer partially dissociates in order to encircle the filament. Encirclement could occur either as concentric dimers or in a daisy chain, where the lasso region of one FH2 domain interacts with the post region of an adjacent FH2. (II) FH2 dimer binds using interactions between the exterior of the dimer and the filament side. Two possible side-binding orientations, as well as a barbed-end-bound dimer, are shown.

(B) Schematic representation of heterogenous dimer formation in velocity analytical ultracentrifucation experiments. If dimer dissociation is appreciable, a heterogeneous dimer should form upon mixing GFP-labeled and unlabeled FH2 domains, resulting in a shift in S value for the GFP signal.

(C) Velocity analytical ultracentrifugation profiles of GFP-INF2-FF (2 μM) alone or mixed with unlabeled INF2-FF (20 μM) or FMNL3-FH2 (20 μM).

coefficient of GFP-INF2-FF shifts appreciably, to a value of 5 S (Figure 4C). This result suggests that the INF2 dimer can dissociate and then reassociate to form the heterogeneous dimer. In contrast, FMNL3 FH2 does not cause an appreciable shift in the sedimentation coefficient of GFP-INF2-FF, suggesting that these dimers cannot efficiently reassociate with each other. These results are similar to those obtained using GFP-INF2-FFC (Table 1) and suggest that the INF2 FH2 domain dimer is capable of dissociating and then reassociating around the filament.

To test directly the binding conformation of INF2 on actin filaments, we imaged complexes of INF2-FFC and actin filaments by negative staining electron microscopy in the presence of beryllium fluoride (a stably bound phosphate analog [33]) and phalloidin. Helical 3D reconstruction of this complex results in a structure at 20 Å resolution. The final reconstruction reveals an inner core of higher density surrounded by an outer region of lower density (Figure 5A). The lower density of the outer region may result from the blurring effect of the variable twist of actin and/or partial occupancy of formin.

The inner core can be fit with a model of filamentous actin structure (PDB 3MFP) on a per protomer basis (Figure 5B). The helical twist per protomer of this reconstructed filament is 166.65°, similar to that of actin alone. However, the helical rise per protomer identified by the program is 28.0 Å, which is 1.5% greater than the 27.6 Å rise of actin alone. Apart from the increased helical rise, the conformation of the protomers does not appear to be altered by INF2-FFC binding at this resolution.

The outer region of lower density is attributed to INF2. This density pattern describes a spiral around the core, at an orientation approximately perpendicular to the filament axis. Part of the density for actin subdomain 1 contributes to the continuity of the spiral. The outer density is at approximately the same position as in a recent crystal structure of an FH2 domain bound to two actin monomers (PDB 4EAH from [31]). When the FH2 portion of this crystal structure is docked into this outer density, it occupies most of the density that does not

correspond to actin (Figure 5B). This conformation encircles the filament. Other conformations in which the FH2 binds without encirclement fit poorly into the outer density. There is a region of unaccounted density close to the C terminus of the fitted FH2 crystal structure. This density may include a portion of the C terminus, which extends 300 residues beyond the FH2, or the FH1 domain.

In principle, this binding configuration would allow for many of the FH2-actin binding interactions observed in the previous crystal structure (PDB 4EAH), including the interaction between INF2's knob helix D and the cleft between actin subdomains 1 and 3. Figure 5C shows a model of the binding pattern based on these structural data. At this resolution, we cannot differentiate between INF2 dimers binding as stacked concentric circles or in a daisy-chain pattern, with oligomerization by lasso/post interactions between adjacent FH2s (Figure 4A).

Discussion

In this work, we elucidate basic features of INF2's actin severing mechanism and propose a working model for severing (Figure 6). INF2 binds filament sides in a manner independent of phosphate release. Side binding occurs through filament encirclement by INF2's FH2 domain, requiring release of at least one FH2-FH2 interaction in the FH2 dimer, which might reassociate or associate with an adjacent FH2. FH2 binding causes a small change in filament rise, but a bigger change might occur upon phosphate release, when the bound FH2 alters filament structure to cause a "weak point" in the filament, making it susceptible to severing. The altered filament structure also enhances the ability of INF2's DAD to bind actin protomers adjacent to the bound FH2. DAD binding further weakens the filament, thus enhancing severing rate. One INF2-FFC dimer is sufficient to carry out this severing reaction.

In our model, as in cofilin-based severing models, the purpose of INF2 is to weaken actin protomer interactions. The thermal motion of the filament then causes breakage at this

Table 1. Velocity Analytical Ultra Analysis of INF2 FH2 Dimer Stability Sedimentation Coefficients

Run	GFP-INF2-FF	GFP-INF2-FFC	+INF2-FF	+FMNL3 FH2	+mDia1 FH2
1	5.33	—	5.03	5.28	—
2	5.48	—	5.07	5.34	—
3	5.38	—	4.92	—	5.28
4		5.73	5.23	5.53	—
5		5.68	5.13	—	—
6		5.63	5.13	—	5.50

Sedimentation coefficient (S) values represented from three individual velocity analytical ultra runs. Results are from multiple experiments tracking either GFP-INF2-FF or GFP-INF2-FFC sedimentation velocity (at 490 nm absorbance) alone or in the presence of unlabeled INF2-FF, FMNL3 FH2 domain, or mDia1 FH2 domain. A plot of run 2 is shown in Figure 4B.

site [34]. INF2 weakens protomer interactions in two ways: by FH2-induced conformational change in filament structure and by DAD binding disrupting protomer-protomer interactions. We will discuss each of the steps below.

Actin Filament Binding by INF2's FH2 Domain

Using electron microscopy, we find that INF2's FH2 domain encircles the actin filament, and through TIRF microscopy, we show that bound dimers have low off rates. Using analytical ultracentrifugation, we show that INF2's FH2 is capable of dissociation and reassociation. Our results do not give an indication of dissociation dynamics, but the fact that we observe both transient and stable GFP-INF2-FFC puncta on filament sides suggests that some binding events are nonproductive. The stability of most GFP-INF2-FFC puncta suggests an extensive interaction, such as encirclement. The resolution of the actin/INF2 electron microscopy (EM) structure presented here is insufficient to determine whether INF2-FFC forms an oligomeric daisy chain similar to Bni1p or binds as independent concentric dimers. Since as few as single GFP-INF2-FFC dimers are capable of severing, oligomerization does not appear to be essential for severing.

Some FH2 domains have been shown to possess the ability to dissociate, including FMNL1, FMNL3, and mDia2, while the FH2 domains of other formins (mDia1 and Bni1p) appear to undergo little dissociation [35, 36]. However, even the apparently stable Bni1p FH2 domain has the ability to encircle actin, as evidenced by the crystal structure of Bni1p-FH2 in an oligomeric chain helically encircling two nonhelical strands of actin monomers [32, 35]. These results suggest that even FH2s that exist as stable dimers in solution might dissociate under some conditions. It is possible that actin filaments might accelerate FH2 dissociation rate to enhance encirclement.

Changes to Filament Structure upon INF2-FH2 Side Binding

We postulate that FH2 binding alters filament structure, resulting in two outcomes: (1) weakening of filament structure, leading to the low but measurable severing by the FF construct and (2) exposure of the DAD binding site on adjacent actin protomers, allowing even greater filament instability. Our EM results show that INF2-FFC induces a small change in filament structure, manifested in a 1.5% change in helical rise. A larger change in filament structure could occur upon phosphate release from the filament, since this causes major changes in filament properties for actin alone [37]. Our EM structure is of INF2-FFC bound to filaments containing the phosphate analog
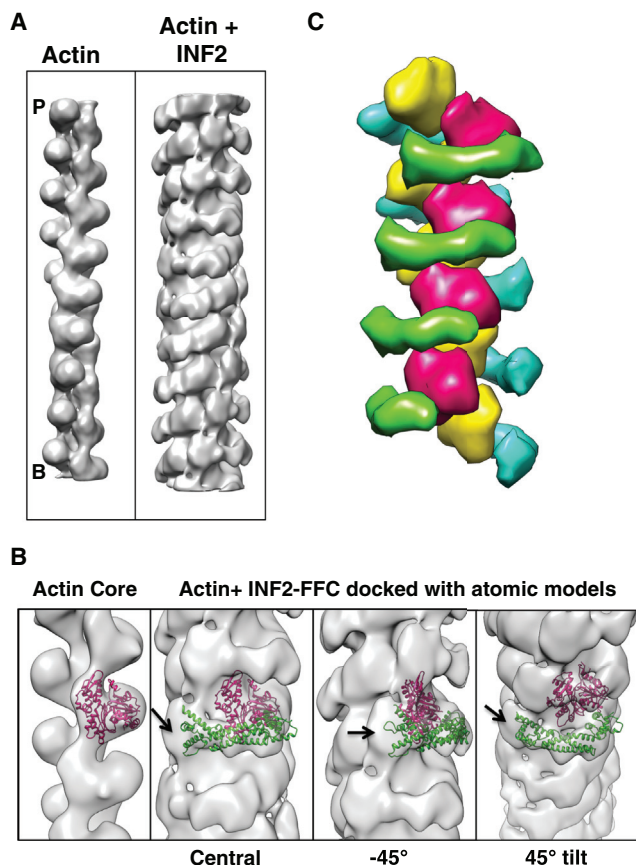

Figure 5. Examination of INF2-FFC Binding Actin Filaments by Electron Microscopy

(A) 3D reconstructions from negative staining EM images of bare (left) and INF2-FFC-bound (right) actin filaments. Barbed (B) and pointed (P) ends are indicated.

(B) Zoomed images of full actin/INF2-FFC reconstruction (inner and outer densities) with actin monomer (PDB 3MFP, pink ribbon) on inner density alone (left panel) or on INF2-bound filaments with FH2 crystal backbone ribbon (PDB 4EAH, green ribbon). Note density unaccounted for by either actin or FH2 (arrow). Three angles are shown.

(C) Schematic model of FH2 (green, blue) binding to filament (red, yellow), based on structural data in agreement with color scheme of [34].

BeF, chosen because of the higher affinity of FFC for filaments versus FF, and the need to prevent severing. Future studies of filament-bound INF2-FF in the presence and absence of phosphate analog, as well as higher-resolution cryoEM reconstruction of the INF2/actin complex, will clarify whether phosphate release causes larger changes in INF2-bound filament structure. For cofilin, filament twist change results from alteration in subdomain 2 and other structural elements of individual actin protomers within cofilin-decorated filaments [23, 25].

DAD Insertion Accelerates Severing

INF2-FFC is at least 40-fold more efficient at severing than INF2-FF, based on our kinetic assays by TIRF microscopy. This increased efficiency is due to the DAD sequence, which binds actin monomers similarly to a WH2 motif. Monomer binding by DAD occurs predominately at the groove between subdomains 1 and 3 at the barbed end of actin, a region that is partially occluded in the filament [8, 38, 39]. In our severing model, the conformational change induced by FH2 binding
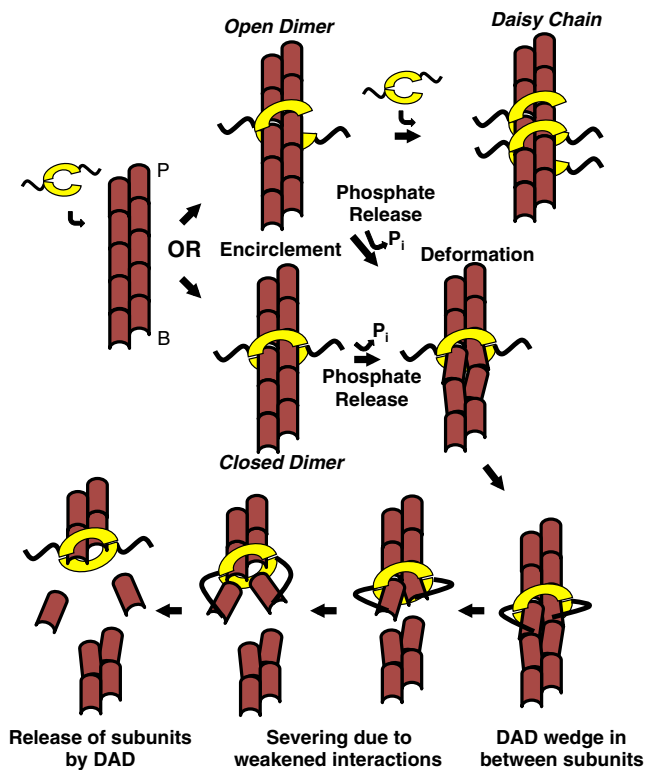
Figure 6. Model of INF2 Severing Mechanism

INF2 dimer partially dissociates and then encircles the filament, either as a closed ring or an open dimer that can form a daisy chain. Subsequent steps are shown in the closed ring conformation, but could also occur as the open dimer. INF2 binding causes a change in helical rise. Upon phosphate release, INF2 causes further local filament deformation, partially exposing the DAD binding site between subdomains 1 and 3 of adjacent actin protomers. DAD binding destabilizes the filament by wedging between protomers. These destabilizations lead to severing at this weak point. Upon severing, INF2 remains bound to the new barbed end, and DAD releases bound actin monomers removed from filament. Our data suggest that DAD binding to the barbed-end side of the FH2 is favored.

serves to increase exposure of the DAD binding site on adjacent actin protomers. DAD binding further disrupts interprotomer contacts and compromises filament stability at this site, leading to severing. Our two-color TIRF studies, showing a higher instance of GFP-INF2-FFC on the new barbed end, suggest that the DAD preferentially binds protomers to the barbed end of the FH2. These experiments also show a variable time between INF2 binding and severing. This lag could suggest that the actual severing event is due to thermal motion of the filament and thus is probabilistic in nature.

A Low Number of INF2 Dimers Can Induce Severing

We frequently observe as few as two GFP molecules in the immediate vicinity of a severing event within 0.5 s of the event, suggesting that a low number of INF2-FFC dimers are sufficient for severing. Due to the noise in our fluorescence calibration (~2-fold), we cannot claim that single FFC dimers are capable of severing. Another source of possible uncertainty in our barbed-end calibration standard is that we have no direct evidence that INF2 binds barbed ends as a dimer, but a large amount of evidence for other formins suggests that this is the case. The dependence of severing on INF2-FFC concentration does not reveal any strong negative cooperativity, with rapid

severing occurring at the highest INF2 concentrations that we are able to test (up to 1 μM). In this feature, INF2 is different from cofilin, for which saturated binding inhibits severing by creating uniform twist [23, 24]. For INF2, small local filament deformations might promote filament instability and severing.

INF2 also presents both similarities and differences to another well-characterized severing protein, gelsolin. Similar to INF2, gelsolin is a barbed-end binding protein that can bind filament sides [40]. Also similar to INF2, gelsolin wraps around the filament, making contacts through several motifs including a WH2-like domain. It is unclear whether one gelsolin molecule is capable of severing. However, gelsolin's severing mechanism might involve long-range changes in filament twist and/or other changes in filament structure [41–43].

INF2 Severing in the Cellular Context

A functional consequence of severing is to produce new filament ends for at least two purposes: (1) priming new filament growth through elongation- or Arp2/3-complex-mediated branched nucleation or (2) creating new filament ends for depolymerization. Both cofilin and gelsolin have been proposed to serve both functions depending on the cellular context [40, 44, 45].

Which function does INF2-mediated severing serve? For the INF2-CAAX variant, severing could be a mechanism for rapidly amplifying filaments number after initial nucleation at the ER/mitochondrial interface [13]. Since constitutively active INF2 causes excessive actin polymerization at mitochondrial fission sites [13], INF2 certainly is a contributor to the assembly of these filaments. Alternately, severing might participate in rapid depolymerization of these filaments at the completion of mitochondrial fission, since these filaments appear to be highly transient. In any case, our results set fundamental parameters for understanding INF2 function in cells by showing that single INF2 dimers are capable of severing and that INF2 binds actin filaments by encirclement.

Experimental Procedures

Detailed plasmid construction, protein purification, buffer composition, and analysis methods can be found in the Supplemental Experimental Procedures. In brief, formins were expressed in Rosetta2 *E. coli* (Stratagene) as GST fusion proteins, following procedures used previously [8].

TIRF Microscopy

Rabbit skeletal muscle actin (1 μM, 20% TAMRA labeled) diluted in TIRF buffer (1× KMEI, 100 mM DTT, 0.2 mM ATP, 15 mM glucose, 0.5% methyl cellulose, 0.01mg/ml catalase [Sigma C3515], 0.05mg/ml glucose oxidase [Sigma G6125], and 0.1% BSA) was polymerized for 7 min in flow chambers, at which point indicated concentrations of formin or cofilin were added. The filaments were visualized on a Nikon Eclipse Ti-E inverted microscope, and simultaneous dual-color images were acquired every 100 ms with TIRF objective (60× 1.49 NA) and two iXON Ultra 897 cameras. Detailed methods can be found in the Supplemental Experimental Procedures.

Velocity Analytical Ultra

Analytical ultracentrifugation was conducted using a Beckman Proteomelab XL-A and an AN-60 rotor. For sedimentation velocity analytical ultracentrifugation, GFP-INF2-FF or GFP-INF2-FFC (2 μM) was mixed with unlabeled INF2-FF or either FMNL3-F or mDIA-F as negative controls (20 μM unlabeled protein) in K100MEIDT and centrifuged at 50,000 rpm with monitoring at 490 nm. Data were analyzed by Sedfit. Sedimentation coefficient reported is that of the major peak (at least 80% of the total analyzed mass) of GFP sedimentation.

Negative Staining Electron Microscopy

For creation of negatively stained grids, actin (bare or INF2-FFC-decorated) samples were applied to EM grids with continuous carbon and were then

stained by 2.5% uranyl acetate solution. Prepared grids were imaged in an FEI Tecnai F20 microscope operated at 200 keV acceleration, and images were taken with a Tietz F415 charge-coupled device (CCD) camera (TVIPS) at 50,000 nominal magnification. Filaments from the CCD frames were manually selected with EMAN [46] *helixboxer* module. Helical 3D reconstructions were conducted with IHRSR [47] with EMAN as the reconstruction engine. Detailed methods can be found in the Supplemental Experimental Procedures.

Supplemental Information

Supplemental Information includes Supplemental Experimental Procedures, three figures, one table, and six movies and can be found with this article online at http://dx.doi.org/10.1016/j.cub.2013.12.018.

References

1. Chhabra, E.S., and Higgs, H.N. (2007). The many faces of actin: matching assembly factors with cellular structures. Nat. Cell Biol. 9, 1110–1121.
2. Moseley, J.B., Sagot, I., Manning, A.L., Xu, Y., Eck, M.J., Pellman, D., and Goode, B.L. (2004). A conserved mechanism for Bni1- and mDia1-induced actin assembly and dual regulation of Bni1 by Bud6 and profilin. Mol. Biol. Cell 15, 896–907.
3. Chesarone, M.A., and Goode, B.L. (2009). Actin nucleation and elongation factors: mechanisms and interplay. Curr. Opin. Cell Biol. 21, 28–37.
4. Paul, A.S., and Pollard, T.D. (2009). Review of the mechanism of processive actin filament elongation by formins. Cell Motil. Cytoskeleton 66, 606–617.
5. Higgs, H.N., and Peterson, K.J. (2005). Phylogenetic analysis of the formin homology 2 domain. Mol. Biol. Cell 16, 1–13.
6. Heimsath, E.G., Jr., and Higgs, H.N. (2012). The C terminus of formin FMNL3 accelerates actin polymerization and contains a WH2 domain-like sequence that binds both monomers and filament barbed ends. J. Biol. Chem. 287, 3087–3098.
7. Gould, C.J., Maiti, S., Michelot, A., Graziano, B.R., Blanchoin, L., and Goode, B.L. (2011). The formin DAD domain plays dual roles in autoinhibition and actin nucleation. Curr. Biol. 21, 384–390.
8. Chhabra, E.S., and Higgs, H.N. (2006). INF2 Is a WASP homology 2 motif-containing formin that severs actin filaments and accelerates both polymerization and depolymerization. J. Biol. Chem. 281, 26754–26767.
9. Ramabhadran, V., Korobova, F., Rahme, G.J., and Higgs, H.N. (2011). Splice variant-specific cellular function of the formin INF2 in maintenance of Golgi architecture. Mol. Biol. Cell 22, 4822–4833.
10. Andrés-Delgado, L., Antón, O.M., Madrid, R., Byrne, J.A., and Alonso, M.A. (2010). Formin INF2 regulates MAL-mediated transport of Lck to the plasma membrane of human T lymphocytes. Blood 116, 5919–5929.
11. Madrid, R., Aranda, J.F., Rodríguez-Fraticelli, A.E., Ventimiglia, L., Andrés-Delgado, L., Shehata, M., Fanayan, S., Shahheydari, H., Gómez, S., Jiménez, A., et al. (2010). The formin INF2 regulates basolateral-to-apical transcytosis and lumen formation in association with Cdc42 and MAL2. Dev. Cell 18, 814–827.
12. Chhabra, E.S., Ramabhadran, V., Gerber, S.A., and Higgs, H.N. (2009). INF2 is an endoplasmic reticulum-associated formin protein. J. Cell Sci. 122, 1430–1440.
13. Korobova, F., Ramabhadran, V., and Higgs, H.N. (2013). An actin-dependent step in mitochondrial fission mediated by the ER-associated formin INF2. Science 339, 464–467.
14. Brown, E.J., Schlöndorff, J.S., Becker, D.J., Tsukaguchi, H., Tonna, S.J., Uscinski, A.L., Higgs, H.N., Henderson, J.M., and Pollak, M.R. (2010). Mutations in the formin gene INF2 cause focal segmental glomerulosclerosis. Nat. Genet. 42, 72–76.
15. Boyer, O., Nevo, F., Plaisier, E., Funalot, B., Gribouval, O., Benoit, G., Cong, E.H., Arrondel, C., Tête, M.J., Montjean, R., et al. (2011). INF2 mutations in Charcot-Marie-Tooth disease with glomerulopathy. N. Engl. J. Med. 365, 2377–2388.
16. Maciver, S.K., Zot, H.G., and Pollard, T.D. (1991). Characterization of actin filament severing by actophorin from Acanthamoeba castellanii. J. Cell Biol. 115, 1611–1620.
17. Hayden, S.M., Miller, P.S., Brauweiler, A., and Bamburg, J.R. (1993). Analysis of the interactions of actin depolymerizing factor with G- and F-actin. Biochemistry 32, 9994–10004.
18. De La Cruz, E.M. (2009). How cofilin severs an actin filament. Biophys. Rev. 1, 51–59.
19. Blanchoin, L., and Pollard, T.D. (2002). Hydrolysis of ATP by polymerized actin depends on the bound divalent cation but not profilin. Biochemistry 41, 597–602.
20. Blanchoin, L., and Pollard, T.D. (1999). Mechanism of interaction of Acanthamoeba actophorin (ADF/Cofilin) with actin filaments. J. Biol. Chem. 274, 15538–15546.
21. Suarez, C., Roland, J., Boujemaa-Paterski, R., Kang, H., McCullough, B.R., Reymann, A.C., Guérin, C., Martiel, J.L., De la Cruz, E.M., and Blanchoin, L. (2011). Cofilin tunes the nucleotide state of actin filaments and severs at bare and decorated segment boundaries. Curr. Biol. 21, 862–868.
22. Carlier, M.F., Pantaloni, D., Evans, J.A., Lambooy, P.K., Korn, E.D., and Webb, M.R. (1988). The hydrolysis of ATP that accompanies actin polymerization is essentially irreversible. FEBS Lett. 235, 211–214.
23. McGough, A., Pope, B., Chiu, W., and Weeds, A. (1997). Cofilin changes the twist of F-actin: implications for actin filament dynamics and cellular function. J. Cell Biol. 138, 771–781.
24. McCullough, B.R., Grintsevich, E.E., Chen, C.K., Kang, H., Hutchison, A.L., Henn, A., Cao, W., Suarez, C., Martiel, J.L., Blanchoin, L., et al. (2011). Cofilin-linked changes in actin filament flexibility promote severing. Biophys. J. 101, 151–159.
25. Galkin, V.E., Orlova, A., Kudryashov, D.S., Solodukhin, A., Reisler, E., Schröder, G.F., and Egelman, E.H. (2011). Remodeling of actin filaments by ADF/cofilin proteins. Proc. Natl. Acad. Sci. USA 108, 20568–20572.
26. Ressad, F., Didry, D., Xia, G.X., Hong, Y., Chua, N.H., Pantaloni, D., and Carlier, M.F. (1998). Kinetic analysis of the interaction of actin-depolymerizing factor (ADF)/cofilin with G- and F-actins. Comparison of plant and human ADFs and effect of phosphorylation. J. Biol. Chem. 273, 20894–20902.
27. Bobkov, A.A., Muhlrad, A., Pavlov, D.A., Kokabi, K., Yilmaz, A., and Reisler, E. (2006). Cooperative effects of cofilin (ADF) on actin structure suggest allosteric mechanism of cofilin function. J. Mol. Biol. 356, 325–334.
28. Pavlov, D., Muhlrad, A., Cooper, J., Wear, M., and Reisler, E. (2007). Actin filament severing by cofilin. J. Mol. Biol. 365, 1350–1358.
29. Andrianantoandro, E., and Pollard, T.D. (2006). Mechanism of actin filament turnover by severing and nucleation at different concentrations of ADF/cofilin. Mol. Cell 24, 13–23.
30. De La Cruz, E.M. (2005). Cofilin binding to muscle and non-muscle actin filaments: isoform-dependent cooperative interactions. J. Mol. Biol. 346, 557–564.
31. Thompson, M.E., Heimsath, E.G., Gauvin, T.J., Higgs, H.N., and Kull, F.J. (2013). FMNL3 FH2-actin structure gives insight into formin-mediated actin nucleation and elongation. Nat. Struct. Mol. Biol. 20, 111–118.
32. Otomo, T., Tomchick, D.R., Otomo, C., Panchal, S.C., Machius, M., and Rosen, M.K. (2005). Structural basis of actin filament nucleation and processive capping by a formin homology 2 domain. Nature 433, 488–494.
33. Combeau, C., and Carlier, M.F. (1988). Probing the mechanism of ATP hydrolysis on F-actin using vanadate and the structural analogs of phosphate BeF-3 and A1F-4. J. Biol. Chem. 263, 17429–17436.
34. Elam, W.A., Kang, H., and De la Cruz, E.M. (2013). Biophysics of actin filament severing by cofilin. FEBS Lett. 587, 1215–1219.

35. Xu, Y.W., Moseley, J.B., Sagot, I., Poy, F., Pellman, D., Goode, B.L., and Eck, M.J. (2004). Crystal structures of a Formin Homology-2 domain reveal a tethered dimer architecture. Cell *116*, 711–723.

36. Harris, E.S., Rouiller, I., Hanein, D., and Higgs, H.N. (2006). Mechanistic differences in actin bundling activity of two mammalian formins, FRL1 and mDia2. J. Biol. Chem. *281*, 14383–14392.

37. Kudryashov, D.S., and Reisler, E. (2013). ATP and ADP actin states. Biopolymers *99*, 245–256.

38. Chereau, D., Kerff, F., Graceffa, P., and Dominguez, R. (2005). Structural basis of the actin-WH2 domain interaction. Biophys. J. *88*, 10A–11A.

39. Chereau, D., Kerff, F., Graceffa, P., Grabarek, Z., Langsetmo, K., and Dominguez, R. (2005). Actin-bound structures of Wiskott-Aldrich syndrome protein (WASP)-homology domain 2 and the implications for filament assembly. Proc. Natl. Acad. Sci. USA *102*, 16644–16649.

40. Nag, S., Larsson, M., Robinson, R.C., and Burtnick, L.D. (2013). Gelsolin: the tail of a molecular gymnast. Cytoskeleton (Hoboken) *70*, 360–384.

41. McGough, A., Chiu, W., and Way, M. (1998). Determination of the gelsolin binding site on F-actin: implications for severing and capping. Biophys. J. *74*, 764–772.

42. Prochniewicz, E., Zhang, Q.N., Janmey, P.A., and Thomas, D.D. (1996). Cooperativity in F-actin: binding of gelsolin at the barbed end affects structure and dynamics of the whole filament. J. Mol. Biol. *260*, 756–766.

43. Orlova, A., Prochniewicz, E., and Egelman, E.H. (1995). Structural dynamics of F-actin: II. Cooperativity in structural transitions. J. Mol. Biol. *245*, 598–607.

44. Chan, A.Y., Bailly, M., Zebda, N., Segall, J.E., and Condeelis, J.S. (2000). Role of cofilin in epidermal growth factor-stimulated actin polymerization and lamellipod protrusion. J. Cell Biol. *148*, 531–542.

45. Bravo-Cordero, J.J., Magalhaes, M.A.O., Eddy, R.J., Hodgson, L., and Condeelis, J. (2013). Functions of cofilin in cell locomotion and invasion. Nat. Rev. Mol. Cell Biol. *14*, 405–415.

46. Ludtke, S.J., Baldwin, P.R., and Chiu, W. (1999). EMAN: semiautomated software for high-resolution single-particle reconstructions. J. Struct. Biol. *128*, 82–97.

47. Egelman, E.H. (2007). The iterative helical real space reconstruction method: surmounting the problems posed by real polymers. J. Struct. Biol. *157*, 83–94.